Comprehensive Evaluation Of Attitude and Orbit Estimation Using Actual Earth Magnetic Field Data

by

Julie K. Deutschmann* and Itzhack Y. Bar-Itzhack+

Abstract

A single, augmented Extended Kalman Filter (EKF), which simultaneously and autonomously estimates spacecraft attitude and orbit has been developed and successfully tested with real magnetometer and gyro data only. Because the earth magnetic field is a function of time and position, and because time is known quite precisely, the differences between the computed and measured magnetic field components, as measured by the magnetometers throughout the entire spacecraft orbit, are a function of both orbit and attitude errors. Thus, conceivably these differences could be used to estimate both orbit and attitude; an observability study validated this assumption. The results of testing the EKF with actual magnetometer and gyro data, from four satellites supported by the NASA Goddard Space Flight Center (GSFC) Guidance, Navigation, and Control Center, are presented and evaluated. They confirm the assumption that a single EKF can estimate both attitude and orbit when using gyros and magnetometers only.

I. INTRODUCTION

Many future low-budget missions, such as the NASA Small and Mid-Size Explorer Series and university class explorers, are looking for inexpensive and autonomous approaches to orbit and attitude estimation. One sensor being considered as a prime is the magnetometer because it is reliable and low cost. For these reasons, magnetometers have been the focus of several recent studies. Emphasis has been placed on using only the magnetometer to separately estimate the spacecraft trajectory[1,2,3] and attitude[4,5]. Studies have also been performed which

---

*Aerospace Engineer. NASA-GSFC Guidance, Navigation, and Control Center, Code 572, Greenbelt, MD 20771, USA. Tel 301-286-9033, Fax 301-286-0369, julie.deutschmann@gsfc.nasa.gov

+Sophie and William Shamban Professor of Aerospace Engineering. Faculty of Aerospace Engineering. Technion-Israel Institute of Technology, Haifa 32000, Israel. Tel +972-4-829-3196, Fax +972-4-823-1848, ibaritz@tx.technion.ac.il

show remarkable accuracy of the magnetometer in estimating attitude when accurate rate information is available[7].

In this work, we present the design and test results of a ***single*** extended Kalman filter and its application to actual data obtained from four satellites; namely, Compton Gamma Ray Observatory (CGRO, NORAD No. 20580), Rossi X-Ray Timing Explorer (RXTE, NORAD No. 23757), the Earth Radiation Budget Satellite (ERBS, NORAD No. 15354), and the Total Ozone Mapping Spectrometer-Explorer Platform (TOMS-EP, NORAD No. 23940). The present work is an extension of the research reported on in Ref. 7 where both attitude and trajectory have been successfully estimated using simulated magnetometer and rate data. In that work large initial errors were applied with a resulting accuracy of 4 km root sum square (RSS) in position and less than 1 degree RSS in attitude.

In the work presented here, we summarize the derivation of the EKF, highlighting the development of the measurement matrix, which constitutes the crucial element in combining the dependence of the magnetic field residuals on both attitude and trajectory estimation errors. The satellites considered here vary in inclination (23 degrees for CGRO to 97 degrees for TOMS-EP) and in size of the magnetometer quantization error (0.3 to 6.4 milliGauss). Comparisons are made with operational estimates of position, velocity, and attitude that were very accurate with respect to the filter generated estimation errors (e.g. CGRO position measurement error was less than 1000 meters and that of ERBS was within 200 meters, etc.). These reference values were computed by NASA Goddard Space Flight Center (GSFC) flight dynamics personnel. We show the ability of the filter to overcome large initial errors and a comparison of the final accuracy achieved with each satellite. This work could prove valuable as a prime trajectory and attitude

estimation system for satellites with coarse accuracy requirements, or as a backup to a prime system in satellites with greater accuracy needs.

II. EXTENDED KALMAN FILTER (EKF) ALGORITHM

For clarity of the developments that will follow we review the special features of the EKF algorithm that was used in this work. The EKF algorithm is based on the following assumed models:

System Model:

$$\dot{\mathbf{X}}(t) = \mathbf{f}(\mathbf{X}(t), t) + \mathbf{w}(t) \tag{1.a}$$

Measurement Model:

$$\mathbf{y}_{k+1} = \mathbf{h}_{k+1}(\mathbf{X}(t_{k+1})) + \mathbf{v}_{k+1} \tag{1.b}$$

where $\mathbf{w}(t)$ is a zero mean white process noise, $\mathbf{v}_{k+1}$ is a zero mean white sequence measurement error, and $\mathbf{X}(t)$ is the state vector. In this work $\mathbf{X}(t)$ is defined as

$$\mathbf{X}^T = [a,\ e,\ i,\ \Omega,\ \omega,\ \theta,\ C_d, \mathbf{b}^T,\ \mathbf{q}^T] \tag{2}$$

The first six elements of $\mathbf{X}(t)$ are the classical Keplerian orbital elements[8,9] which determine the spacecraft orbit, position and velocity; namely, the semi-major axis (a), eccentricity (e), inclination (i), right ascension of the ascending node (Ω), argument of perigee (ω), and true anomaly (θ). C_d is the drag coefficient, $\mathbf{b}$ is a vector of the on board gyro constant drift rates, and $\mathbf{q}$ represents the attitude quaternion.

The EKF used in this work is a unified filter that consists of an orbital part and an attitude part. Thus Eqs. (1) are written as

$$\begin{bmatrix} \dot{\mathbf{X}}_o \\ \dot{\mathbf{X}}_a \end{bmatrix} = \begin{bmatrix} \mathbf{f}_o(\mathbf{X}_o(t), t) \\ \mathbf{f}_a(\mathbf{X}_a(t), t) \end{bmatrix} + \begin{bmatrix} \mathbf{w}_o \\ \mathbf{w}_a \end{bmatrix} \tag{3.a}$$

and

$$\mathbf{y}_{k+1} = \mathbf{h}_{k+1}(\mathbf{X}_o(t_{k+1}), \mathbf{X}_a(t_{k+1})) + \mathbf{v}_{k+1} \tag{3.b}$$

where

$$\mathbf{X}_o^T = [a, e, i, \Omega, \omega, \theta, C_d] \tag{4.a}$$

and

$$\mathbf{X}_a^T = [\mathbf{b}^T, \mathbf{q}^T] \tag{4.b}$$

The processes, which are applied in order to derive the linearized dynamics and measurement models used in the EKF, treat the orbital and the attitude parts differently according to the specific physical natures of each part. The difference in treatment is expressed in the development of the measurement model as well as in the development of the dynamics model. The development of the orbital part of the measurement model is done by the customary partial differentiation, $\partial \mathbf{h} / \partial \mathbf{X}_o$, which yields a Jacobian matrix[10] whereas, as will be explained later, the attitude part is done using the *perturbation method.* Similarly, in the development of the orbital part of the dynamics matrix, the customary partial differentiation yields the Jacobian matrix $\partial \mathbf{f}_o / \partial \mathbf{X}_o$. However, as will be shown later, the development of the dynamics model that describes the evolution of the attitude error between measurement updates is done entirely different.

The state vector usually consists of three kinds of states; those that describe the dynamics of the system, those that are augmented due to the nonwhite nature of the stochastic processes that drive the dynamics model, and those that are augmented due to the same in the measurement noise. In our case the states $a, e, i, \Omega, \omega,$ and θ that appear in $\mathbf{X}$ of Eq. (2) are states that describe the system dynamics. The state C_d is a non-white state driving the dynamics model, which was augmented via the state augmentation procedure. Similarly $\mathbf{q}$ is a state vector that describes the dynamics whereas $\mathbf{b}$, the gyro bias state vector that drives $\mathbf{q}$, is non-white, and as such is also augmented into the state vector. Sometimes it is also necessary to describe the measurement error

as a combination of white noise and colored noise[1], which, as mentioned before, results in further augmentation of the non-white vector into the state vector. However in our filter this was not necessary.

We now proceed to describe the measurement update stage and the propagation stage of the EKF algorithm used in this work.

II.1 EKF Measurement Update

The measurement update of the state estimate and of the estimation error covariance are performed, respectively, as

$$\hat{\mathbf{X}}_{k+1}(+) = \hat{\mathbf{X}}_{k+1}(-) + \mathrm{K}_{k+1}[\mathbf{y}_{k+1} - \mathbf{h}_{k+1}(\hat{\mathbf{X}}_{k+1}(-))] \tag{5.a}$$

$$\mathrm{P}_{k+1}(+) = [\mathrm{I} - \mathrm{K}_{k+1}\mathrm{H}_{k+1}]\mathrm{P}_{k+1}(-)[\mathrm{I} - \mathrm{K}_{k+1}\mathrm{H}_{k+1}]^{\mathrm{T}} + \mathrm{K}_{k+1}\mathrm{R}_{k+1}\mathrm{K}_{k+1}^{\mathrm{T}} \tag{5.b}$$

where $(-)$ denotes the a-priori value and $(+)$ denotes the a-posteriori value, and K_{k+1} is the Kalman gain computed according to

$$\mathrm{K}_{k+1} = \mathrm{P}_{k+1}(-)\mathrm{H}_{k+1}^{\mathrm{T}}[\mathrm{H}_{k+1}\mathrm{P}_{k+1}(-)\mathrm{H}_{k+1}^{\mathrm{T}} + \mathrm{R}_{k+1}]^{-1} \tag{6}$$

where

$$\mathrm{H}_{k+1} = [\mathrm{H}_{\mathrm{o}} \mid \mathrm{H}_{\mathrm{a}}]_{k+1} \tag{7}$$

and where H_{o} is the orbit part of the measurement matrix, and H_{a} is the attitude part. The matrix P_{k+1} is the estimation error covariance matrix, and R_{k+1} is the covariance matrix of the zero mean white sequence $\mathbf{v}_{k+1}$.

Let us denote $\mathbf{y}_{k+1} - \mathbf{h}_{k+1}(\hat{\mathbf{X}}_{k+1}(-))$ of Eq. (5.a) by $\mathbf{z}_{k+1}$. The latter is the data, which is used by the EKF to update the a-priori state estimate. This data, which is called *effective measurement*,

is the difference between the measurement and the estimate of the measurement. Therefore in our case the data, $\mathbf{z}_{k+1}$, used by the filter is computed as

$$\mathbf{z}_{k+1} = \mathbf{B}_{m,k+1} - \mathbf{B}(\hat{\mathbf{X}}_{k+1}(-), t_{k+1}) \tag{8}$$

here $\mathbf{B}_{m,k+1}$ is the magnetic field vector measured by the magnetometer, $\mathbf{B}(\hat{\mathbf{X}}_{k+1}(-), t_{k+1})$ is the estimated magnetic field vector as a function of the estimated state at time t_{k+1} computed using a 10^{th} order International Geomagnetic Reference Field (IGRF) model.

Define $\mathbf{x}_{k+1}$ as the difference between the true state vector $\mathbf{X}_{k+1}$ and its estimate; that is,

$$\mathbf{x}_{k+1}^T = [\delta a, \delta e, \delta i, \delta\Omega, \delta\omega, \delta\theta, \delta C_d, \delta\mathbf{b}^T, \boldsymbol{\alpha}^T]_{k+1} \tag{9}$$

A comparison between **X**, defined in Eq. (2), and **x**, defined in the last equation, reveals that other than **q**, the latter is a perturbation of the former. In **x** the expression for **q** is replaced by $\boldsymbol{\alpha}$. This is done because, as will be shown later, in the EKF update stage we express the attitude error by a vector of small angles, $\boldsymbol{\alpha}$, whereas in the propagation stage we express the attitude by the quaternion **q**. We use $\mathbf{z}_{k+1}$, [Eq. (8)], to update the estimate, $\hat{\mathbf{x}}_{k+1}$ of $\mathbf{x}_{k+1}$ as follows

$$\hat{\mathbf{x}}_{k+1} = \mathrm{K}_{k+1}\mathbf{z}_{k+1} \tag{10}$$

The updated vector, $\hat{\mathbf{x}}_{k+1}$, is used to update the a-priori state estimate, $\hat{\mathbf{X}}_{k+1}(-)$, as follows

$$\hat{\mathbf{X}}_{k+1}(+) = \mathbf{g}\left(\hat{\mathbf{X}}_{k+1}(-), \hat{\mathbf{x}}_{k+1}\right) \tag{11}$$

The nature of **g** will be explained shortly.

Development of the measurement matrix

Figure 1 shows the geometry of the magnetic field vector. The U coordinates are earth fixed coordinates and the I are inertial coordinates. Both coordinate systems are fixed to the earth

center. The Magnetic field vector is expressed in the magnetic spherical coordinates, F, as follows $\mathbf{B}_F^T = [B_r, B_{\theta B}, B_{\phi B}]$. Begin the development of the measurement matrix using the perturbation technique, by writing the estimated magnetic field at the spacecraft location as

$$\mathbf{B}(\hat{\mathbf{X}}, t) = \hat{D}_b^I \hat{D}_I^F \hat{\mathbf{B}}_F + \mathbf{v}' \tag{12}$$

where $\hat{\mathbf{B}}_F$ is computed using the IGRF magnetic field model, the estimated position and time, $\hat{D}_I^F$ is the estimated transformation matrix that transforms from magnetic spherical to inertial coordinates, $\hat{D}_b^I$ is the estimated attitude matrix which transforms the estimated magnetic field vector from the inertial to the body coordinate system, and $\mathbf{v}'$ is the magnetic field model error. (Note that we consider the situation at time point t_{k+1}; however we drop the subscript k+1 for clarity). On the other hand, the measured magnetic field vector, as measured by the magnetometer, can be written as

$$\mathbf{B}_m = D_b^I D_I^F \mathbf{B}_F + \mathbf{v}_m \tag{13}$$

where $\mathbf{B}_F$ is the correct magnetic field vector in magnetic spherical coordinates, D_I^F is the correct transformation from the magnetic spherical to the inertial coordinates, D_b^I is the true transformation from inertial to body coordinates, and $\mathbf{v}_m$ is the magnetometer measurement error.

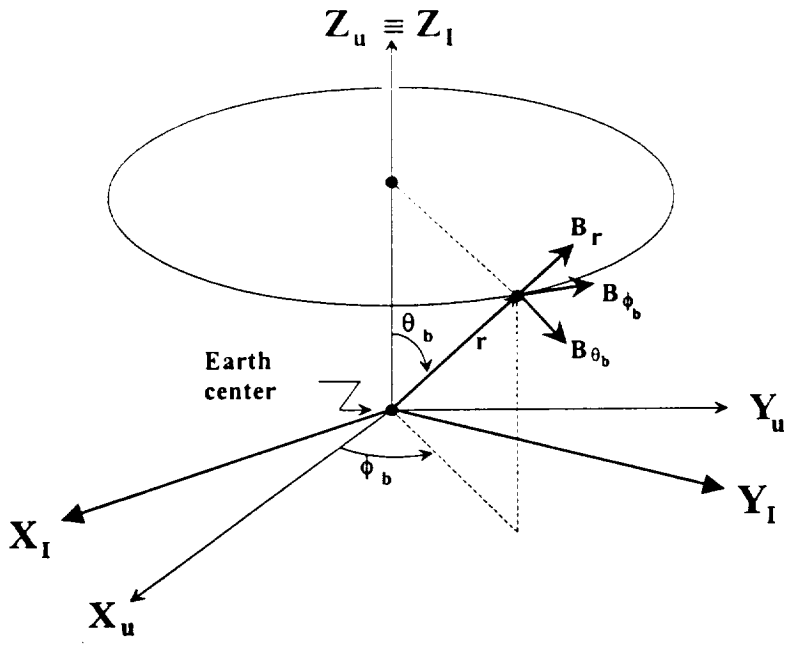

Fig. 1: Definition of the magnetic spherical coordinates

The effective measurement, **z**, is defined as follows.

$$\mathbf{z} = \mathbf{B}_m - \mathbf{B}(\hat{\mathbf{X}}(-), t) = D_b^I D_I^F \mathbf{B}_F + \mathbf{v}_m - \hat{D}_b^I \hat{D}_I^F \hat{\mathbf{B}}_F - \mathbf{v}' \tag{14}$$

Write the transformation of $\hat{\mathbf{B}}_F$ to the estimated body coordinates as

$$\hat{D}_b^I \hat{D}_I^F \hat{\mathbf{B}}_F = D_b^I D_I^F \mathbf{B}_F + \Delta(D_b^I D_I^F \mathbf{B}_F) \tag{15}$$

where $\Delta(D_b^I D_I^F \mathbf{B}_F)$ is the error in the estimation of the magnetic field vector resolved in the body axes. Define

$$\mathbf{v} = \mathbf{v}_m - \mathbf{v}' \tag{16}$$

Using the last two equations, Eq. (15) becomes

$$\mathbf{z} = \Delta(D_b^I D_I^F \mathbf{B}_F) + \mathbf{v} \tag{17}$$

Now

$$\Delta(D_b^I D_I^F \mathbf{B}_F) = \Delta D_b^I (D_I^F \mathbf{B}_F) + D_b^I \Delta(D_I^F \mathbf{B}_F) \tag{18}$$

The second term on the right hand side of Eq. (18) is the part of the effective measurement caused by errors in the orbital states. This term can be developed into $H_o \mathbf{x}_o$ where H_o is the

measurement matrix for the orbital states and $\mathbf{x}_o$ denotes the orbital error states, which are the first seven elements of $\mathbf{x}$, that are defined in Eq. (9). The derivation of $H_o\mathbf{x}_o$ is given in Ref. 10 where H_o was developed using partial differentiation

$$H_o = \left.\frac{\partial \mathbf{h}(\mathbf{X}_o, \mathbf{X}_a)}{\partial \mathbf{X}_o}\right|_{\mathbf{X}=\hat{\mathbf{X}}} \tag{19}$$

The expansion of the first term leads to the measurement matrix for the attitude states. Rewrite that term as

$$\Delta D_b^I (D_I^F \mathbf{B}_F) = \Delta D_b^I \mathbf{B}_I \tag{20}$$

where $\mathbf{B}_I$ is the computed magnetic field vector in inertial coordinates. We define ΔD_b^I, the error in the transformation, as the difference between the *correct* body coordinates and the *computed* (estimated) body coordinate system. The computed coordinates are determined by the computed (estimated) transformation matrix, $\hat{D}_b^I$, which is the transformation from the inertial to the computed (rather than the correct) body coordinate system. We write it as

$$\hat{D}_b^I = D_c^I = D_c^b D_b^I \tag{21}$$

so

$$\Delta D_b^I = \hat{D}_b^I - D_b^I = D_c^b D_b^I - D_b^I \tag{22}$$

For small attitude errors we can assume that the matrix D_c^b is composed of small angles, thus

$$D_c^b = I - \begin{bmatrix} 0 & -\psi & \vartheta \\ \psi & 0 & -\varphi \\ -\vartheta & \varphi & 0 \end{bmatrix} = I - [\boldsymbol{\alpha}\times] \tag{23}$$

where $[\boldsymbol{\alpha}\times]$ is the cross product matrix of $\boldsymbol{\alpha}$ defined in the last equation, and where $\boldsymbol{\alpha}^T = [\varphi, \vartheta, \psi]$. The vector $\boldsymbol{\alpha}$ is a vector of three small Euler angles describing the attitude difference between the true and estimated attitudes. These errors are defined about the body x, y, and z axes respectively. Using Eq. (23) in Eq. (22) yields

$$\Delta D_b^I = (I - [\alpha \times])D_b^I - D_b^I = -[\alpha \times]D_b^I \tag{24}$$

Substituting Eq. (24) into the first term on the right-hand side of Eq. (18) yields

$$\Delta D_b^I(D_I^F \mathbf{B}_F) = -[\alpha \times]D_b^I \mathbf{B}_I = -[\alpha \times]\mathbf{B}_b = [\mathbf{B}_b \times]\alpha \tag{25}$$

Following the last equation we substitute the first term of Eq. (18) by $[\mathbf{B}_b \times]\alpha$ and, following earlier discussion, the second term by $H_o \mathbf{x}_o$. Substituting the result into Eq. (17) yields

$$\mathbf{z} = [\mathbf{B}_b \times]\alpha + H_o \mathbf{x}_o + \mathbf{v} \tag{26}$$

The error state, $\mathbf{x}$, is composed of the orbital error states denoted by $\mathbf{x}_o$, the error in estimating the gyro bias, $\delta\mathbf{b}$, and the vector of small angular errors in the attitude, α (see Eq. 9). Therefore, in order to relate $\mathbf{z}$ to $\mathbf{x}$ we need to introduce a matrix that relates $\delta\mathbf{b}$ to $\mathbf{z}$. However, $\delta\mathbf{b}$ has no direct influence on $\mathbf{z}$, therefore we can write Eq. (26) as

$$\mathbf{z} = [H_o \mid 0_{3\times3} \mid [\mathbf{B}_b \times]]\,\mathbf{x} + \mathbf{v} \tag{27}$$

where $0_{3\times3}$ is a 3×3 zero matrix. (Note that $\mathbf{b}$ is introduced into the state vector, $\mathbf{X}$, because it is a non-white vector driving the attitude. In order to comply with the requirement of the KF that the driving force be white, $\mathbf{b}$ is augmented with the original state vector. This is a well-known standard procedure. The existence of $\mathbf{b}$ in $\mathbf{X}$ results in the existence of $\delta\mathbf{b}$ in $\mathbf{x}$.) Following Eq. (27), the combined measurement matrix is given as

$$H = [H_o \mid 0_{3\times3} \mid [\mathbf{B}_b \times]] = [H_o \mid H_a] \tag{28}$$

where $H_a = [0_{3\times3_b} \mid [\mathbf{B}_b \times]]$. Because $\mathbf{B}_b$ is not known, $\mathbf{B}_m$, the magnetic field vector measured by the magnetometer, is used instead, thus

$$H_a = [0_{3\times3} \mid [\mathbf{B}_m \times]] \tag{29}$$

An explicit expression for H_o is given in Ref. 10 using partial differentiation.

We realize that a new state vector, $\boldsymbol{\alpha}$, has emerged in the development of the measurement matrix. This vector of angular errors expresses the attitude error between the true and estimated attitude. We will show shortly that this vector will easily blend with the orbital error states. Using Eqs. (26) and (27), the effective measurement at time t_{k+1} is written as

$$\mathbf{z}_{k+1} = H_{k+1}\mathbf{x}_{k+1} + \mathbf{v}_{k+1} \tag{30}$$

where

$$\mathbf{x}^T_{k+1} = [\delta a, \delta e, \delta i, \delta\Omega, \delta\omega, \delta\theta, \delta C_d, \delta\mathbf{b}^T, \boldsymbol{\alpha}^T]_{k+1} \tag{31}$$

Define

$$\mathbf{x}^T_{o,k+1} = [\delta a, \delta e, \delta i, \delta\Omega, \delta\omega, \delta\theta, \delta C_d]_{k+1} \tag{32}$$

from Eqs. (31) and (32) it is obvious that

$$\mathbf{x}^T_{k+1} = [\mathbf{x}^T_{o,k+1}, \delta\mathbf{b}^T, \boldsymbol{\alpha}^T_{k+1}] \tag{33}$$

Similar to $\mathbf{x}^T_{o,k+1}$, define

$$\mathbf{X}^T_{o,k+1} = [a, e, i, \Omega, \omega, \theta, C_d]_{k+1} \tag{34}$$

then from Eqs. (2) and (4) we obtain

$$\mathbf{X}^T_{k+1} = [\mathbf{X}^T_{o,k+1}, \mathbf{b}^T, \mathbf{q}^T_{k+1}] \tag{35}$$

With Eq. (35) we can now explain the nature of $\mathbf{g}$ in Eq. (11). Indeed, the update of the state vector estimate is a function of both $\hat{\mathbf{X}}_{k+1}(-)$ and $\hat{\mathbf{x}}_{k+1}$ which is computed using Eq. (9). While the orbital and the gyro bias parts of $\hat{\mathbf{X}}_{k+1}(-)$ are updated additively as follows

$$\begin{bmatrix} \hat{\mathbf{X}}_{o,k+1}(+) \\ \hat{\mathbf{b}}_{k+1}(+) \end{bmatrix} = \begin{bmatrix} \hat{\mathbf{X}}_{o,k+1}(-) \\ \hat{\mathbf{b}}_{k+1}(-) \end{bmatrix} + \begin{bmatrix} \hat{\mathbf{x}}_{o,k+1} \\ \delta\hat{\mathbf{b}}_{k+1} \end{bmatrix} \tag{36}$$

the attitude part is updated multiplicatively as described next. It is well known that the three small angles in the vector, $\hat{\boldsymbol{\alpha}}$, can be used to construct a quaternion $d\hat{\mathbf{q}}$ as follows[11]

$$d\hat{\mathbf{q}}^T = [\tfrac{1}{2}\hat{\varphi}, \tfrac{1}{2}\hat{\vartheta}, \tfrac{1}{2}\hat{\psi}, 1] = [\tfrac{1}{2}\hat{\boldsymbol{\alpha}}^T, 1] \tag{37}$$

where $d\hat{\mathbf{q}}$ is the estimate of $d\mathbf{q}$ which expresses the small attitude difference between our best estimate of the attitude and the correct attitude. In other word, if one rotates the correct coordinate system, whose orientation is expressed by $\mathbf{q}_{k+1}$, through the rotation expressed by $d\mathbf{q}$, one reaches the current (a-priori) estimate of the orientation expressed by $\hat{\mathbf{q}}_{k+1}(-)$. This is represented by

$$\hat{\mathbf{q}}_{k+1}(-) = \mathbf{q}_{k+1} \otimes d\mathbf{q}_{k+1} \tag{38}$$

where $\otimes$ denotes a quaternion product. Post-multiplying Eq.(38) by the inverse of $d\mathbf{q}_{k+1}$ yields

$$\mathbf{q}_{k+1} = \hat{\mathbf{q}}_{k+1}(-) \otimes d\mathbf{q}_{k+1}^{-1} \tag{39.a}$$

If $d\mathbf{q}_{k+1}$ is known precisely then the operation $\hat{\mathbf{q}}_{k+1}(-) \otimes d\mathbf{q}_{k+1}^{-1}$ yields $\mathbf{q}_{k+1}$, but because we have only an estimate, $d\hat{\mathbf{q}}_{k+1}$, of $d\mathbf{q}_{k+1}$ the product $\hat{\mathbf{q}}_{k+1}(-) \otimes d\hat{\mathbf{q}}_{k+1}^{-1}$ yields only the estimate of $\mathbf{q}_{k+1}$. Because $d\hat{\mathbf{q}}_{k+1}$ is the a-posteriori estimate of $d\mathbf{q}_{k+1}$, this new estimate of $\mathbf{q}_{k+1}$ is the a-posteriori estimate. In other words

$$\hat{\mathbf{q}}_{k+1}(+) = \hat{\mathbf{q}}_{k+1}(-) \otimes d\hat{\mathbf{q}}_{k+1}^{-1} \tag{39.b}$$

The last equation can be viewed as a correction to $\hat{\mathbf{q}}_{k+1}(-)$ which yields $\hat{\mathbf{q}}_{k+1}(+)$. In order to assure the normality of the quaternion, normalization is performed at this stage, which yields

$$\hat{\mathbf{q}}_{k+1}(+) = \hat{\mathbf{q}}_{k+1}(+) / \left|\hat{\mathbf{q}}_{k+1}(+)\right| \tag{39.c}$$

Following Eq. (35) the full updated state vector is given by

$$\hat{\mathbf{X}}_{k+1}^{T}(+) = [\hat{\mathbf{X}}_{o,k+1}^{T}(+), \hat{\mathbf{b}}_{k+1}^{T}, \hat{\mathbf{q}}_{k+1}^{T}(+)] \tag{40}$$

II.2 EKF Propagation

Recall the dynamics equation (3.a)

$$\begin{bmatrix} \dot{\mathbf{X}}_o \\ \dot{\mathbf{X}}_a \end{bmatrix} = \begin{bmatrix} \mathbf{f}_o(\mathbf{X}_o(t), t) \\ \mathbf{f}_a(\mathbf{X}_a(t), t) \end{bmatrix} + \begin{bmatrix} \mathbf{w}_o \\ \mathbf{w}_a \end{bmatrix} \tag{3.a}$$

The propagation of the covariance is given as

$$P_{k+1}(-) = A_k(\mathbf{X}_k(+))P_k(+)A_k^T(\mathbf{X}_k(+)) + Q_k \tag{41}$$

where Q_k is the spectral density matrix of $\mathbf{w}(t)$ and A_k is the approximated transition matrix. A_k is computed using the following first order Taylor series expansion

$$A_k = I + F_k \cdot \Delta T \tag{42}$$

where ΔT is the time interval between gyro measurements. As described earlier, the dynamics matrix of the orbit part is obtained by computing the Jacobian $F_{o,k}$ as follows

$$F_{o,k} = \left.\frac{\partial \mathbf{f}(\mathbf{X}_o(t), t)}{\partial \mathbf{X}}\right|_{\mathbf{X} = \hat{\mathbf{X}}_k(-)} \tag{43}$$

The actual computation of $F_{o,k}$ is based on the orbital dynamics equations, given in the ensuing.

Based on Eq. (1), the propagation of the state estimate, is performed by solving the differential equation

$$\dot{\hat{\mathbf{X}}}(t) = \mathbf{f}(\hat{\mathbf{X}}(t), t) \tag{44}$$

The updated estimate of the state vector, $\hat{\mathbf{X}}_k(+)$ serves as the initial condition of the solution, and the final solution at time t_{k+1} is $\hat{\mathbf{X}}_{k+1}(-)$. The dynamics equation (44) consists of the orbital dynamics equation, which in our case, is non-linear, and the attitude kinematics, which is linear.

II.2.1 Nominal Dynamics

Orbital Dynamics

The orbital dynamics describe the motion of a mass point in a central force field including drag[12]. There are several possibilities to describe the orbital dynamics. The most natural possibility is by position, velocity and acceleration expressed in a Cartesian coordinate system. The advantage of this choice is in its ability to handle orbits which are completely circular but its disadvantage is in the fast change of the state that describes the dynamics. This in turn requires an increased computational load. One can also choose equinoctial variables[13] to describe the orbital dynamics. This choice too enables the handling of completely circular orbits. Moreover, all but one variable of the equinoctial variables change slowly [see Ref. 9, p. 143]. Finally, one can use Keplerian parameters, which, similarly to the equinoctial variables, include only one fast varying parameter. Although these parameters cannot describe perfectly circular orbits, as will be seen later, they can handle nearly circular orbits. For this reason and because Keplerian parameters are widely used and well understood we chose them for the present study.

The differential equations for each of the orbital elements of the state vector **X**, including the drag coefficient are given as[10]

$$\dot{x}_1 = \dot{a} = \frac{2a}{r}(2a - r)\frac{f_t}{V} \tag{45.a}$$

$$\dot{x}_2 = \dot{e} = \frac{2f_t}{V}(\cos\theta + e) + \frac{f_n}{V}\frac{r}{a}\sin\theta \tag{45.b}$$

$$\dot{x}_3 = \dot{i} = \frac{rf_h}{h}\cos\theta^* \tag{45.c}$$

$$\dot{x}_4 = \dot{\Omega} = \frac{rf_h}{h \cdot \sin i}\sin\theta^* \tag{45.d}$$

$$\dot{x}_5 = \dot{\omega} = \frac{1}{e}[\frac{2f_t}{V}\sin\theta - \frac{f_n}{V}(2e + \frac{r}{a}\cos\theta)] - \dot{\Omega}\cos i \qquad (45.e)$$

$$\dot{x}_6 = \dot{\theta} = \frac{h}{r^2} - \dot{\Omega}\cos i - \dot{\omega} \qquad (45.f)$$

$$\dot{x}_7 = \dot{C}_d = 0 \qquad (45.g)$$

where f_t, f_n and f_h are the along track, radial, and cross track perturbing accelerations due to the effect of drag, and where

$$\theta^* = \omega + \theta \qquad (46.a)$$

$$h = \sqrt{\mu_E a(1-e^2)} \qquad (46.b)$$

$$r = \frac{a(1-e^2)}{1+e\cos\theta} \qquad (46.c)$$

$$V = \sqrt{2\mu_E(\frac{1}{r} - \frac{1}{2a})} \qquad (46.d)$$

and μ_E is the earth gravitation constant.

Attitude Dynamics

The linear differential equation governing the dynamics of the attitude quaternion is given by

$$\dot{\mathbf{q}} = \frac{1}{2}\tilde{\Omega}\mathbf{q} \qquad (47.a)$$

where $\tilde{\Omega}$ is a 4x4 skew-symmetric matrix containing the elements of the spacecraft rate vector as measured by the gyros[11]. We assume that the gyros have bias, and using the state augmentation approach[14], mentioned in Section II, the three bias states were included in the state vector (Eqs. (2) and (4.b)). The bias states model is

$$\dot{\mathbf{b}} = 0 \qquad (47.b)$$

It should be mentioned here that although the correct modeling of bias is as shown in Eq. (47.b), we added white driving noise for filter stability[15].

II.2.2 Error-State Dynamics

Orbital Error-State Dynamics

The error dynamics model can be written as follows

$$F = \begin{bmatrix} F_o & 0 \\ 0 & F_a \end{bmatrix} \tag{48}$$

where F_o is the orbital part and F_a is the attitude part of the error state dynamics. From Eq. (32) it is obvious that the dimension of F_o is 7×7. The elements of this matrix are obtained when applying the partial differentiation of Eq. (43) to Eqs. (45). In the case where the drag coefficient, C_d, is not being estimated and the effect of J_2 is neglected, the non-zero elements of F_o are as follows[10]. Let

$$f_6 = \frac{\sqrt{\mu_E}(1 + e \cdot \cos\theta)^2}{[a(1-e^2)]^{3/2}} \tag{49}$$

then

$$f_{a6,1} = -\frac{3}{2a} f_6(\mathbf{X}) \qquad (50.a) \qquad f_{a6,2} = \left[\frac{3e}{1-e^2} + \frac{2\cos\theta}{1 + e \cdot \cos\theta}\right] f_6(\mathbf{X}) \qquad (50.b)$$

$$f_{a6,6} = -\frac{2e \cdot \sin\theta}{1 + e \cdot \cos\theta} f_6(\mathbf{X}) \tag{50.c}$$

In the more general case where C_d and the influence of J_2 are considered, the development of F_o is more lengthy and is found in Refs. 10 and 11.

Attitude Error-State Dynamics

As mentioned earlier, the development of F_1, the dynamics model that describes the evolution of the attitude and gyro bias errors between measurement updates, is done entirely differently than that of F_0. From Eq. (37)

$$d\mathbf{q}^T = [\tfrac{1}{2}\boldsymbol{\alpha}^T, 1] \tag{51}$$

Generalization of the relation expressed in Eq. (38) yields

$$\hat{\mathbf{q}} = \mathbf{q} \otimes d\mathbf{q} \tag{52}$$

from which we obtain

$$\dot{\hat{\mathbf{q}}} = \dot{\mathbf{q}} \otimes d\mathbf{q} + \mathbf{q} \otimes d\dot{\mathbf{q}} \tag{53}$$

Noting that $\mathbf{q}^{-1} \otimes \mathbf{q} = \mathbf{u}$, where $\mathbf{u}$ is the unity quaternion, we get from the last equation

$$d\dot{\mathbf{q}} = \mathbf{q}^{-1} \otimes \dot{\hat{\mathbf{q}}} - \mathbf{q}^{-1} \otimes \dot{\mathbf{q}} \otimes d\mathbf{q} \tag{54}$$

We can replace $\dot{\mathbf{q}}$ by $\frac{1}{2}\mathbf{q} \otimes \tilde{\boldsymbol{\omega}}$, where $\tilde{\boldsymbol{\omega}}$ is $\boldsymbol{\omega}$ presented in quaternion form [see Ref 16], and similarly $\dot{\hat{\mathbf{q}}}$ by $\frac{1}{2}\hat{\mathbf{q}} \otimes \tilde{\boldsymbol{\omega}}_m$, where $\tilde{\boldsymbol{\omega}}_m$ is the measured angular rate, $\boldsymbol{\omega}_m$, presented also in quaternion form. The last equation then becomes

$$d\dot{\mathbf{q}} = \mathbf{q}^{-1} \otimes \tfrac{1}{2}\hat{\mathbf{q}} \otimes \tilde{\boldsymbol{\omega}}_m - \mathbf{q}^{-1} \otimes \tfrac{1}{2}\mathbf{q} \otimes \tilde{\boldsymbol{\omega}} \otimes d\mathbf{q} \tag{55}$$

Using Eq. (52) as well as the relation $\boldsymbol{\omega}_m = \boldsymbol{\omega} + d\boldsymbol{\omega}$ (where $d\boldsymbol{\omega}$ is the angular rate measurement error, which, in our case, is the gyro drift rate) Eq. (55) can be written as

$$d\dot{\mathbf{q}} = \mathbf{q}^{-1} \otimes \tfrac{1}{2}\mathbf{q} \otimes d\mathbf{q} \otimes (\tilde{\boldsymbol{\omega}} + d\tilde{\boldsymbol{\omega}}) - \mathbf{q}^{-1} \otimes \tfrac{1}{2}\mathbf{q} \otimes \tilde{\boldsymbol{\omega}} \otimes d\mathbf{q} \tag{56}$$

Eq. (56) can be written as

$$d\dot{\mathbf{q}} = \tfrac{1}{2}[d\mathbf{q} \otimes \tilde{\boldsymbol{\omega}} - \tilde{\boldsymbol{\omega}} \otimes d\mathbf{q}] + \tfrac{1}{2} d\mathbf{q} \otimes d\tilde{\boldsymbol{\omega}} \tag{57}$$

Using the rules of quaternion multiplication [see e.g. Ref. 11, p. 759], the real part of the quaternion $[d\mathbf{q} \otimes \tilde{\boldsymbol{\omega}} - \tilde{\boldsymbol{\omega}} \otimes d\mathbf{q}]$ is identically zero; that is

$$[\mathbf{dq} \otimes \tilde{\boldsymbol{\omega}} - \tilde{\boldsymbol{\omega}} \otimes \mathbf{dq}]_r = 0 \tag{58.a}$$

where r denotes the real part. Similarly we find that

$$[\mathbf{dq} \otimes \mathbf{d}\tilde{\boldsymbol{\omega}}]_r = -\mathbf{d}\boldsymbol{\omega} \cdot \tfrac{1}{2}\boldsymbol{\alpha} \approx 0 \tag{58.b}$$

where $\mathbf{d}\boldsymbol{\omega}$ is a vector. For the imaginary part of the quaternion $[\mathbf{dq} \otimes \tilde{\boldsymbol{\omega}} - \tilde{\boldsymbol{\omega}} \otimes \mathbf{dq}]$ we find that

$$[\mathbf{dq} \otimes \tilde{\boldsymbol{\omega}} - \tilde{\boldsymbol{\omega}} \otimes \mathbf{dq}]_{Im} = 2\boldsymbol{\omega} \times \tfrac{1}{2}\boldsymbol{\alpha} \tag{59.a}$$

where Im denotes the imaginary part, and $\boldsymbol{\omega}$ is a vector. For the imaginary part of the quaternion $[\mathbf{dq} \otimes \mathbf{d}\tilde{\boldsymbol{\omega}}]$ we find that

$$[\mathbf{dq} \otimes \mathbf{d}\tilde{\boldsymbol{\omega}}]_{Im} = \mathbf{d}\boldsymbol{\omega} + \mathbf{d}\boldsymbol{\omega} \times \tfrac{1}{2}\boldsymbol{\alpha} \approx \mathbf{d}\boldsymbol{\omega} \tag{59.b}$$

Using Eqs. (58) and (59), Eq. (57) becomes

$$\dot{\boldsymbol{\alpha}} = \boldsymbol{\omega} \times \boldsymbol{\alpha} + \mathbf{d}\boldsymbol{\omega} \tag{60.a}$$

The term $\mathbf{d}\boldsymbol{\omega}$ is the error introduced by the gyros, which we assume it consists of two parts: a very low frequency signal, and a wide band signal. We modeled the former as bias and the latter as white noise; thus

$$\mathbf{d}\boldsymbol{\omega} = \mathbf{b} + \mathbf{n} \tag{60.b}$$

where **b** is the bias state whose model was given in Eq. (47.b). As mentioned earlier, **b** was augmented with the original state vector (see Eq. 2). In the error state vector, **x**, defined in Eq. (10), the error in estimating **b** is denoted $\delta\mathbf{b}$ where obviously

$$\delta\dot{\mathbf{b}} = 0 \tag{60.c}$$

The resulting matrix, F_a, describes the propagation of $\hat{\boldsymbol{\alpha}}$ as well as the estimate of the gyro constant drift rate. It is a 6×6 matrix. In view of Eq. (60) the non-zero elements of F_a are as follows.

$$f_{a4,1} = 1 \quad (61.a) \qquad f_{a4,5} = \omega_z \quad (61.b) \qquad f_{a4,6} = -\omega_y \quad (61.c)$$

$f_{a5,2} = 1$ (61.d) $f_{a5,4} = -\omega_z$ (61.e) $f_{a5,6} = \omega_x$ (61.g)

$f_{a6,3} = 1$ (61.h) $f_{a6,4} = \omega_y$ (61.i) $f_{a6,5} = -\omega_x$ (61.j)

III. FILTER TESTING

The observability of the unified filter was examined first using the following analysis. Let us denote the transition matrix, which corresponds to F of Eq. (48), by $A_k(\hat{\mathbf{X}})$. This matrix transforms $\mathbf{x}_{k-1}$, the error in the state estimate at time t_{k-1}, to $\mathbf{x}_k$ the error in the state estimate at time t_k. If at a certain time point t_m, the initial error in the state estimate, denoted by $\mathbf{x}_0$, can be computed then for our purposes the system is observable. This is so because in the EKF, $\mathbf{x}$ is defined as the difference between the system state vector, $\mathbf{X}$ and its ***known*** estimate, $\hat{\mathbf{X}}$. Adopting the common approach to the proof of complete observability of a discrete linear system, we express the first m measurements as follows

$$\mathbf{y}_j = H_j\left[\prod_{i=0}^{j} A_i(\hat{\mathbf{X}})\right]\mathbf{x}_0 \qquad j = 0, 1, ..., m-1 \tag{62}$$

where $A_0(\hat{\mathbf{X}}) = I$. Form the matrix equation

$$\begin{bmatrix} \mathbf{y}_0 \\ \mathbf{y}_1 \\ \mathbf{y}_2 \\ \cdot \\ \cdot \\ \mathbf{y}_{m-1} \end{bmatrix} = \begin{bmatrix} H_0 \\ H_1A_1(\hat{\mathbf{X}}) \\ H_2A_2(\hat{\mathbf{X}})A_1(\hat{\mathbf{X}}) \\ \cdot \\ \cdot \\ H_{m-1}A_{m-1}(\hat{\mathbf{X}})\cdots A_1(\hat{\mathbf{X}}) \end{bmatrix}\mathbf{x}_0 \tag{63}$$

If there are n independent rows in the right hand side matrix (the observability matrix) in Eq. (63) then, of course, $\mathbf{x}_0$ can be computed, hence the state is observable. Testing the filter with

CGRO data, it was found that after 5 measurements there were 13 independent rows in the observability matrix, and because the size of the state vector was 13, the system was observable.

After finding that the filter operated on an observable CGRO system, the EKF algorithm described in the preceding was tested on data obtained from four satellites. The four satellites were, CGRO, RXTE, ERBS, and TOMS. The launch dates of these satellites and the start time of the data used in the testing is presented in Table I. The satellites varied in altitude,

Table I. Satellite Launch Times

Satellite	Launch Date	Start of Data
RXTE	Dec. 30, 1995	1996, Sept. 8, 19h 53min. 11.769sec
ERBS	Oct. 5, 1984	1984, Dec. 25, 19h 22min. 12.000sec
CGRO	April 5, 1991	1993, May 3, 14h 12min. 36.841sec
TOMS	July 2, 1996	1997, March 15, 19h 5min. 14.514sec

inclination, resolution of the telemetry of the magnetometer data (quantization error), and frequency at which the magnetometer telemetry was received. Table II summarizes these

Table II. Satellite Information

Satellite	h (km)	i (deg)	Error (mG)	ΔT (sec)
RXTE	580	23.0	0.3	2
ERBS	614	57	6.4	16
CGRO	340	28.5	0.3	3-4
TOMS	483	97	4	33-34

variations, where h is the average altitude (the orbits were nearly circular), i is the inclination, 'Error' is the quantization error of the telemetry, and ΔT is the time between magnetometer

measurements. In addition, the accuracy of the gyroscopes varied. (Note that the gyro data was needed for computing the attitude dynamics model of Eqs. 47.a and 61.) The CGRO and RXTE gyros were considerably more accurate than those of TOMS and ERBS. (CGRO used the Teledyne DRIRU-II gyro whose drift rate stability was 0.003 degrees per hour over six hours. RXTE used the Kearfott SKIRU-DII which was equivalent to the DRIRU-II gyro. TOMS and ERBS used less accurate gyros whose drift rate stability was about an order of magnitude larger). The initial estimate of each satellite position, velocity and attitude determines the initial orbital parameters and the initial quaternion, which constitute the initial state estimate.

Table III. Initial RSS Errors

Satellite	Position (km)	Velocity (km/sec)	Attitude (deg)
RXTE	2617	2.6	15.7
ERBS	1000	1.1	11.4
CGRO	1098	1.1	12.9
TOMS	2389	2.6	14

The initial estimation errors were determined by comparing the filter position, velocity, and attitude with estimates of position, velocity, and attitude computed by NASA GSFC flight dynamics personnel. The initial errors, which correspond to the initial estimate chosen for each satellite are given in Table III. The errors displayed are the RSS errors.

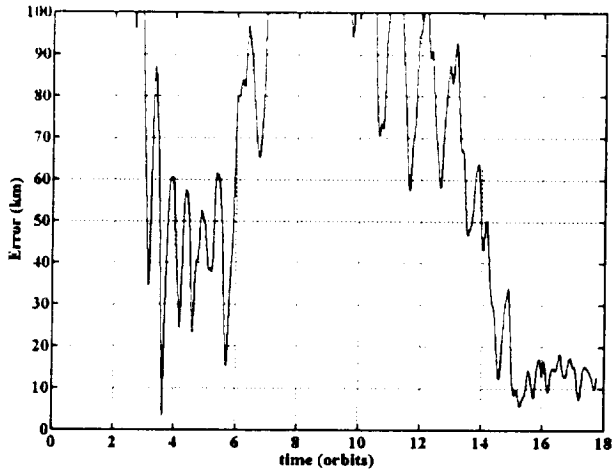

Fig. 2: The Evolution of the RXTE RSS Position Estimation Error.
(From Initial Error of 2617 km).

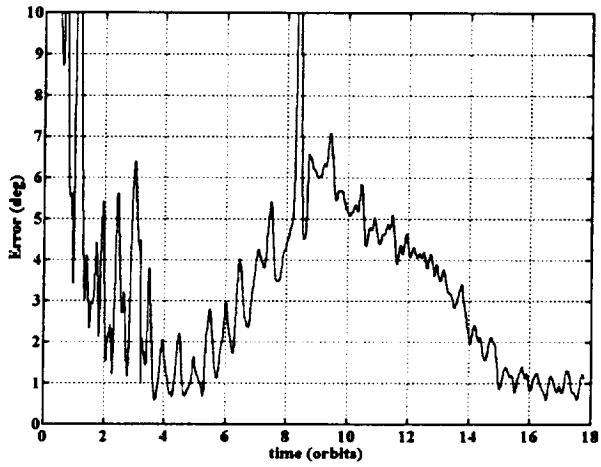

Fig. 3: The Evolution of the RXTE RSS Attitude Estimation Error.
(From Initial Error of 15.7 deg).

The figures presented here show the evolution of the position and attitude estimation errors for each of the four satellites. Figures 2 and 3 show, respectively, the RXTE RSS position and attitude errors, Figs. 4 and 5 show ERBS results, Figs. 6 and 7 show the CGRO results, and finally, TOMS results are presented in Figs. 8 and 9. The velocity errors are not shown, but for each satellite they have a shape similar to the position error.

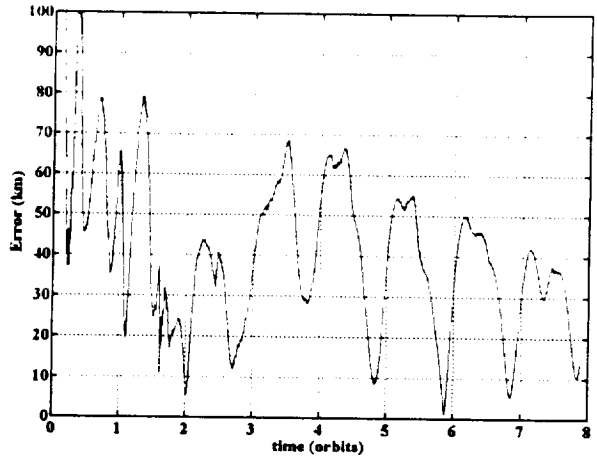

Fig. 4: The Evolution of the ERBS RSS Position Estimation Error. (From Initial Error of 1000 km).

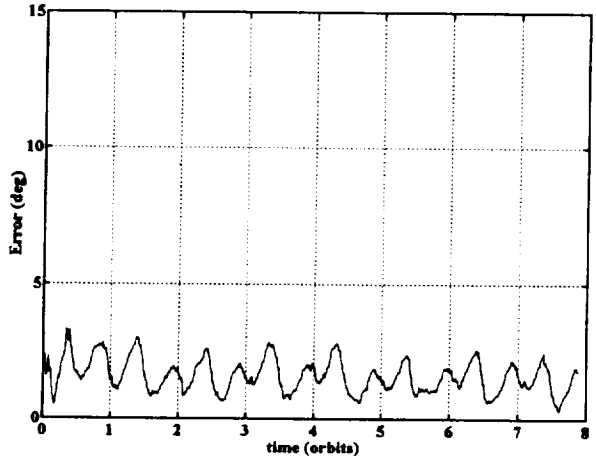

Fig. 5: The Evolution of the ERBS RSS Attitude Estimation Error. (From Initial Error of 11.4 deg).

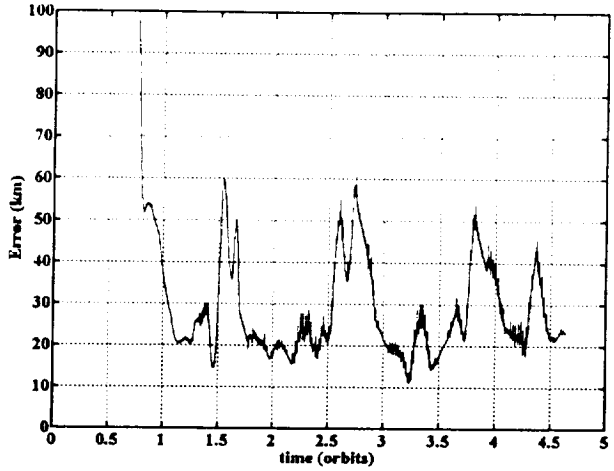

Fig. 6: The Evolution of the CGRO RSS Position Estimation Error. (From Initial Error of 1098 km).

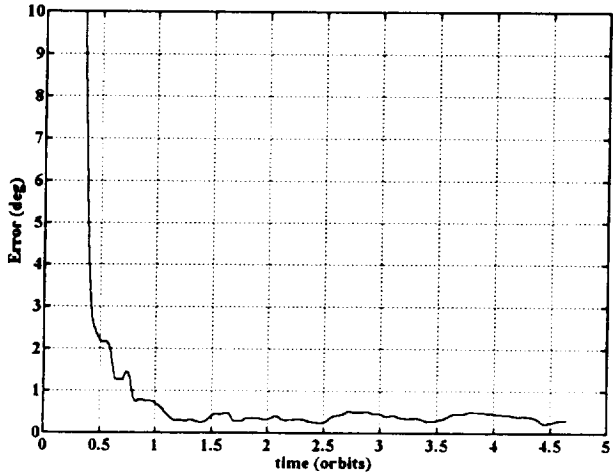

Fig. 7: The Evolution of the CGRO RSS Attitude Estimation Error. (From Initial Error of 12.9 deg).

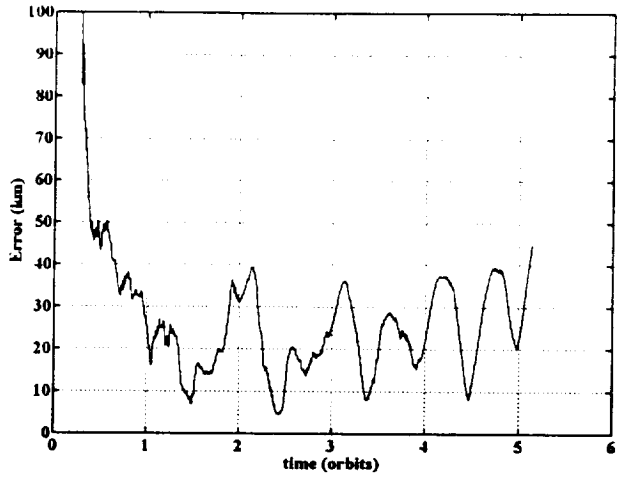

Fig. 8: The Evolution of the TOMS RSS Position Estimation Error.
(From Initial Error of 2389 km).

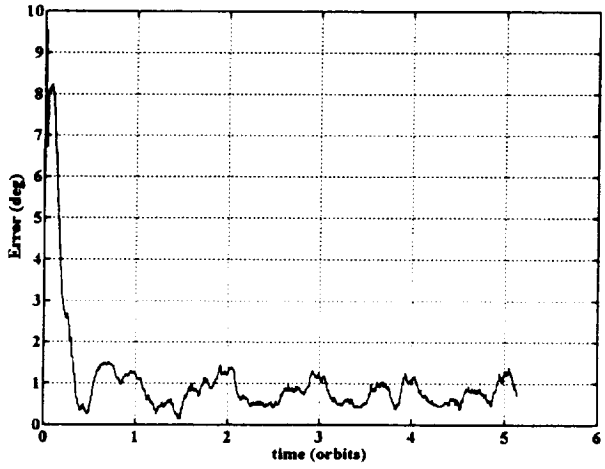

Fig. 9: The Evolution of the TOMS RSS Attitude Estimation Error.
(From Initial Error of 14 deg).

Table IV, summarizes the average RSS errors for position, velocity, and attitude for each satellite (excluding transients). Note that the RXTE transients last for 15 orbits therefore the RXTE RSS errors are averaged only over the last 3 orbits. For ERBS, CGRO, and TOMS

Table IV: Average, RSS Errors (excluding transient effects)

Satellite	Position (km)	Velocity (km/sec)	Attitude (deg)
RXTE*	15	0.015	1.0
ERBS	25	0.03	1.4
CGRO	20	0.02	0.2
TOMS	20	0.025	0.75

*Averages are for the last 3 orbits.

the final position errors are comparable, with averages of 20 to 30 km. All three also converge quickly, including TOMS which started with a 2389 km position error. The position estimates from all three appear to still be converging. However, in order to assure convergence for all four satellites, data of one more earth revolution inside the orbit was necessary. That is, data of some additional 16 orbits was required. Unfortunately the data spans that were available for these satellites were limited. However, the resemblance of the results to results obtained via simulations where, of course, data was not limited, confirm the convergence of the results with real data.

CGRO has the lowest attitude error. The final average RSS attitude error is 0.2 deg. The CGRO data was extensively calibrated prior to its use, the magnetometer quantization error was small and the measurement frequency, particularly of the gyro data was high (0.256 sec between

gyro readings). Surprisingly, the TOMS attitude errors were also relatively small, with a final average of 0.75 degrees. This was a result of the high inclination for TOMS, which resulted in good observability, despite the large quantization error, the low measurement frequency, and the un-calibrated magnetometer data. ERBS had the highest attitude error, with a final average of 1.4 deg. This was because ERBS had the largest quantization error and also a low measurement frequency.

RXTE took considerably longer to converge, and both the attitude and position error results show a divergence in the middle of the span. It is noted that RXTE underwent three attitude maneuvers during this span, which apparently led to a deviation in the drag coefficient, which then led to the increased errors. Once the drag coefficient converged again, the position results improved and for the last 3 orbits were very good with an average RSS position error of approximately 15 km. The final average RSS attitude errors were approximately 1 degree. The RXTE data was not calibrated at all and contains unknown and uncompensated disturbances, which contributed to the larger final attitude error.

These results compare favorably with results obtained in Ref. 17 where only magnetometers were used. In particular the present results fit the accuracy predicted in that reference. They also fit results reported in Ref. 18, which were obtained with simulated data and are better than the results presented in Reference 19.

The gyros that were used on board these spacecraft were well calibrated, therefore their bias was negligible. Consequently the gyro bias states were deactivated; however, in order to examine the ability of the filter to estimate bias, an artificial bias of 1.0 mrad/sec was added to the CGRO gyro output and the filter was re-run with active bias states. The bias states were estimated

without corrupting the estimation of the other states. Figure 10 presents the time history of the estimated bias versus its correct value in the three body axes.

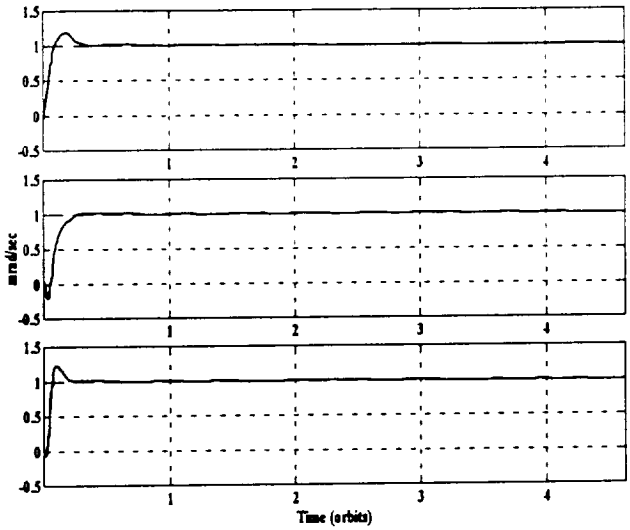

Fig 10: The CGRO Artificial Bias Estimates as a Function of Time (Orbits)

While successful in estimating the larger part of the gyro bias, the filter was unable to estimate very low gyro bias values, apparently because of the large measurement noise. Moreover, when the bias states were activated and the bias to be estimated was negligible, the orbit and attitude estimates degraded considerably. On the other hand, in the presence of large gyro bias, the inclusion of the bias states in the filter was imperative to obtain good orbit and attitude estimates. A byproduct of this inclusion was the estimation of the major part of the gyro bias. The degradation in performance of the filter, when the bias states of the estimator were activated despite the lack of actual bias, has been explained before by the Information Dilution Theorem[20].

IV. CONCLUSIONS

This paper presented a new unified EKF algorithm for estimating spacecraft orbit and attitude based on measurements of the magnetic field and the angular velocity of the spacecraft. To test this algorithm, it was first established that the system, which the EKF had to estimate, was indeed observable for at least the CGRO satellite. Next, magnetometer data and gyro data from four satellites were processed by the EKF. All four converged to final averages of 15 - 30 km in position, 0.015 - 0.03 km/sec in velocity, and 0.2 - 1.5 degrees in attitude (all RSS). Additional results indicated that the EKF could converge from extremely large initial position and velocity errors; CGRO and TOMS, for example, overcame initial position errors exceeding 5000 km.

The data from each of the satellites differed in quantization error and measurement frequency, and the satellites were at 4 different inclinations. The higher inclinations for ERBS and TOMS resulted in quick convergence, and for TOMS gave good final results despite inaccuracies in the data and a large time between measurements. The coarse quantization of the ERBS telemetry and the infrequency of the measurements resulted in the lowest accuracy. On the other hand, the extensive calibration of the CGRO data, the small quantization errors, and the high data frequency contributed to the quick convergence and the higher accuracy achieved with CGRO. It was observed that RXTE required more time to converge, with good final results in position. The RXTE magnetometer data contained disturbances that were not calibrated and hence contributed to the errors in attitude.

Although the filter was designed to also estimate gyro bias, in our experiments we deactivated the bias states because the available gyro data had been calibrated (which removed the gyro bias). In order to test the filter performance when gyro bias is present, artificial gyro bias was added to the CGRO data and the filter bias states were activated. It was found that the filter estimated the

gyro bias without degrading the quality of the attitude and orbit estimation. The filter successfully estimated the larger part of the gyro bias, but was unable to estimate very low gyro bias values, probably because of the large measurement noise. Moreover, when trying to estimate negligible gyro drifts, the orbit and attitude estimates degraded considerably. However, in the presence of large gyro bias, it was necessary to activate the bias states in the filter in order to obtain good orbit and attitude estimates. A byproduct of this inclusion was the estimation of the major part of the gyro bias.

In summary it was shown that magnetometer and gyro measurements on board low earth-orbiting satellites are sufficient for coarse orbit as well as attitude determination when processed by the single EKF, which was developed in this work.

References

[1] Shorshi, G. and Bar-Itzhack, I.Y., "Satellite Autonomous Navigation Based on Magnetic Field Measurements", Journal of Guidance, Control, and Dynamics, Vol. 18, No. 4, 1995, pp. 843-850.

[2] Ketchum, E., "Autonomous Spacecraft Orbit Determination Using the Magnetic Field and Attitude Information", Paper No. AAS 96-005, proceedings of the 19th Annual AAS Guidance and Control Conference, Breckenridge, Colorado, February 1996.

[3] Psiaki, M.L., "Autonomous Orbit and Magnetic Field Determination Using Magnetometer and Star Sensor Data", *Journal of Guidance, Control, and Dynamics*, Vol. 18, No. 3, 1995, pp. 584-592.

[4] Challa, M., Natanson, G., Deutschmann, J. and Galal, K., "A PC-Based Magnetometer-Only Attitude and Rate Determination System for Gyroless Spacecraft", Paper No. 07, presented at the GSFC Flight Mechanics/Estimation Theory Symposium 1995, NASA GSFC, Greenbelt, Maryland, May 16-18, 1995.

[5] Psiaki, M.L., Martel, F., and Pal, P.K. "Three-Axis Attitude Determination via Kalman Filtering of Magnetometer Data", *Journal of Guidance, Control, and Dynamics*, Vol. 14, No. 3, 1990, pp. 506-514.

[6] Hashmall, J., Liu, K. and Rokni, M., "Accurate Spacecraft Attitudes from Magnetometer Data", Paper No. MS95/007, *CNES Int'l Symposium on Space Dynamics*, Toulouse, France, June 19-23, 1995.

[7] Deutschmann, J.K. and Bar-Itzhack, I.Y, "Attitude and Trajectory Estimation Using Earth Magnetic Field Data", Paper No. AIAA-96-3631, *AIAA/AAS Astrodynamics Specialists Conference*, San Diego, CA, July 29-31, 1996.

[8] Bate, R., Mueller and White, J., *Fundamentals of Astrodynamics*, Dover Publications, Inc., New York, NY, 1971, p. 58-60.

[9] Vallado, D.A., *Fundamentals of Astrodynamics and Applications*, McGraw-Hill, New York, NY, 1997, p. 130-139.

[10] Shorshi, G. and Bar-Itzhack, I.Y., "Satellite Autonomous Navigation Based on Magnetic Field Measurements", TAE No. 714, Technion-Israel Institute of Tech., Haifa, Israel, April 1994.

[11] Wertz, J.R., *Spacecraft Attitude Determination and Control*, D. Reidel Publishing Company, Dordrecht, Holland, 1984.

[12] Kaplan, M.H., *Modern Spacecraft Dynamics & Control*, John Wiley & Sons, New York, 1976.

[13] Battin, R.H., *An Introduction to The Mathematics and Methods of Astrodynamics*, AIAA Education Series, New York, 1987, p. 492.

[14] Gelb, A., *Applied Optimal Estimation*, MIT Press, Cambridge MA, 1988. P, 143.

[15] Bryson, A.E., Jr., "Kalman Filter Divergence and Aircraft Motion Estimators", *Journal of Guidance and Control*, Vol. 1, No. 1, 1978, pp. 71-79.

[16] Wicox, J.C., "A New Algorithm for Strap-Down Inertial Navigation," *IEEE Transactions on Aerospace and Electronic Systems*, Vol. AES-3, No. 5, 1967, pp. 796-802.

[17] Psiaki, M.L., Huang, L., and Fox, S.M. "Ground Tests of Magnetometer-Based Autonomous Navigation (MAGNAV) for Low-Earth-Orbiting Satellites", *Journal of Guidance, Control, and Dynamics*, Vol. 16, No. 1, 1993, pp. 206-214.

[18] Deutschmann, J.K., Harman, R.R., and Bar-Itzhack, I.Y., "An innovative Method for Low Cost, Autonomous Navigation for Low Earth Orbit Satellites", Paper No. AIAA-98-4183, *AIAA/AAS Astrodynamics Specialists Conference*, Boston, MA, August 10-12, 1998.

[19] Weigand, M., "Autonomous Satellite Navigation via Kalman Filtering of Magnetometer Data," *Acta Astronautica*, Vol. 38, Nos. 4-8, 1996, pp. 395-403.

[30] Rapoport, I., and Bar-Itzhack, I.Y., "On the Information Dilution Theorem", *Proceedings of the 39th Israel Annual Conference on Aerospace Sciences*, Tel-Aviv and Haifa, Israel, February 17-18, 1999, pp. 205-214.